# Singular value decomposition methods for wave propagation analysis

O. Santolík, Michel Parrot, François Lefeuvre

# Singular value decomposition methods for wave propagation analysis

O. Santolík,[1] M. Parrot, and F. Lefeuvre

Laboratoire de Physique et Chimie de l'Environnement, Centre National de la Recherche Scientifique, Orléans, France

Received 13 July 2000; revised 29 May 2002; accepted 4 September 2002; published 12 February 2003.

[1] We describe several newly developed methods for propagation analysis of electromagnetic plasma waves. We make use of singular value decomposition (SVD) technique and we determine the wave vector direction, ellipticity and directions of axes of the polarization ellipse, wave refractive index, transfer function of electric antennas, estimators of the planarity of polarization, and electromagnetic planarity. Simulations of Z-mode waves, which simultaneously propagate with different wave vectors, indicate that the SVD methods give reasonable results even if the assumption on the presence of a single plane wave is invalid. Simulations of whistler mode waves show that these methods can be used to recognize cases when the waves simultaneously propagate with wave vectors in two opposite hemispheres. Finally, we show an example of analysis of natural whistler mode and Z-mode emissions measured in the high-altitude auroral region by the MEMO experiment onboard the INTERBALL spacecraft. *INDEX TERMS:* 0694 Electromagnetics: Instrumentation and techniques; 6984 Radio Science: Waves in plasma; 2772 Magnetospheric Physics: Plasma waves and instabilities; 2794 Magnetospheric Physics: Instruments and techniques; 0689 Electromagnetics: Wave propagation (4275); *KEYWORDS:* wave propagation, singular value decomposition

**Citation:** Santolík, O., M. Parrot, and F. Lefeuvre, Singular value decomposition methods for wave propagation analysis, *Radio Sci.*, *38*(1), 1010, doi:10.1029/2000RS002523, 2003.

## 1. Introduction

[2] Today's instrumentation for wave measurements in space often allows us to work with multicomponent data [e.g., *Lefeuvre et al.*, 1998; *Gurnett et al.*, 1995; *Cornilleau-Wehrlin et al.*, 1997]. In these devices, full magnetic field vector is measured by three orthogonal antennas, and the electric field is simultaneously measured by at least two electric antennas. With these data, the classical analysis of power spectra and spectrograms can be completed by examination of wave propagation properties. If we suppose the presence of a single plane wave at frequency $f$, the wave vector $\boldsymbol{k}$ can be determined from the linearized Faraday's law:

$$\boldsymbol{k} \times \boldsymbol{E} = \omega \boldsymbol{B}, \tag{1}$$

where $\omega$ is the angular frequency $\omega = 2\pi f$, and $\boldsymbol{E}$ and $\boldsymbol{B}$ are the vectors of complex amplitudes of electric and magnetic fields. Here we suppose that the corresponding analytic signals at a point $\boldsymbol{x}$ can be written as $\Upsilon \exp[\iota(\omega t - \boldsymbol{k} \cdot \boldsymbol{x})]$, where $\iota$ is $\sqrt{-1}$, and $\Upsilon$ stands for $\boldsymbol{E}$ or $\boldsymbol{B}$, respectively.

[3] From (1) it follows that $\boldsymbol{B}$ is always perpendicular to both wave vector and $\boldsymbol{E}$. The perpendicularity to the wave vector is also a consequence of another Maxwell equation, $\boldsymbol{k} \cdot \boldsymbol{B} = 0$. This can be used to determine the wave vector direction, for instance by the minimum variance analysis of magnetic fluctuations [e.g., *Rezeau et al.*, 1993]. This method directly works with waveforms of measured signals. The direction of minimum variance can be attributed to the wave vector direction and the hodographs of the magnetic field plotted in the plane perpendicular to this direction can show the wave polarization. This supposes that the signal is narrow-band or that the wave vector direction does not change with the frequency.

[4] Another way to determine the wave vector directions is based on the multidimensional spectral analysis. This technique acts as a narrow-band frequency filter centered at each analyzed frequency and gives us the power-spectral densities of the measured components and their relative phase and coherency relations. Several different methods to determine propagation characteristics using this information exist in the literature [*Means*, 1972; *McPherron et al.*, 1972; *Samson*, 1973; *Samson and Olson*,

[1]Now at Faculty of Mathematics and Physics, Charles University, Prague, Czech Republic, and Institute of Atmospheric Physics, Czech Academy of Sciences, Prague, Czech Republic.


0048-6604/03/2000RS002523

1980]. All of them are based on the multidimensional spectral analysis of a single vector of field fluctuations, and as far as we know, all known practical applications of these methods concern the magnetic field vector. More recently, *Ladreiter et al.* [1995] developed a method to estimate the propagation parameters of radio waves from the electric field measurements using the singular value decomposition (SVD). Their technique is based on determination of parameters of a theoretical model for the results of the multidimensional spectral analysis, and uses the SVD to improve the minimization procedure.

[5] The multidimensional spectral analysis is the basis of the method we are going to discuss in the present paper. We will show that it is useful and easy to take into account all the information obtained from this analysis of either a single measured vector, or of the simultaneously measured magnetic and electric field data. Based on the SVD, we have developed a new method which is very easy to implement using SVD procedures accessible from numerical libraries. This new technique is essentially different from the method of *Ladreiter et al.* [1995] and the basic idea is presented for the magnetic field data in section 2. We will also show that the new method provides us with some other useful polarization parameters such as the ellipticity, planarity, and the direction of the polarization ellipse axes. Next, we will demonstrate that the method is easily extensible to simultaneously process the electric and magnetic fields (section 3), and that this approach allows us to obtain not only the fully defined wave vector direction, but also the wave number and electromagnetic planarity. Section 4 shows several examples of the analysis results for well defined simulated data, and, finally, section 5 presents an example of the analysis of natural VLF emissions in the high-altitude auroral region.

## 2. Singular Value Decomposition of the Magnetic Spectral Matrix

[6] There are several possible methods of spectral analysis resulting in estimates $\hat{\boldsymbol{B}}(f)$ and $\hat{\boldsymbol{E}}(f)$ of vectors of complex amplitudes of magnetic and electric fields as a function of frequency. For instance, we can use the discrete Fourier transform implemented by the fast Fourier transform algorithm (FFT), and different weighting windows can be used for the time series of real samples (for details, see *Priestley* [1989]). A simple example of discrete Fourier transform method is shown in algebraic calculations in Appendices A and B. Another possibility is to use estimates based on the wavelet analysis.

[7] Using the estimates of magnetic complex amplitudes at a given frequency $f$ (we do not explicitly express functions of $f$ in the following), a hermitian spectral matrix is formed,

$$\hat{S}_{ij} = \langle \hat{B}_i \hat{B}_j^* \rangle \tag{2}$$

where indices $i$ and $j$ stand for the three cartesian components of the magnetic field, * means the complex conjugate, symbols $\langle\ \rangle$ mean average of results obtained from successive time intervals, where estimates $\hat{\boldsymbol{B}}$ are calculated from finite time series of real samples. For a detailed discussion of the multidimensional spectral analysis see [e.g., *Priestley*, 1989]. Note also that this kind of analysis can be implemented in the on-board software of today's space instruments [*Cornilleau-Wehrlin et al.*, 1997].

[8] From (1) it follows that $\boldsymbol{B}$ (a three-dimensional complex vector of magnetic field amplitudes) is perpendicular to the wave vector $\boldsymbol{k}$. This can be expressed by a complex equation,

$$\boldsymbol{B} \cdot \boldsymbol{k} = 0. \tag{3}$$

This equation is at the same time a consequence of the fact that the magnetic field vectors have zero divergence. If we multiply (3) successively by the three cartesian components of $\boldsymbol{B}^*$, we have three mutually dependent equations

$$\sum_{i=1}^{3} B_i B_j^* k_i = 0, \quad j = 1 \ldots 3, \tag{4}$$

where terms $B_i B_j^*$ can be written as components $S_{ij}$ of a spectral matrix of the analytic signals used in (1),

$$S_{ij} = B_i B_j^*. \tag{5}$$

Note that, compared to (2), we have dropped the averaging operation since it has no effect on the components of this idealized spectral matrix.

[9] The three complex equations (4) thus can be rewritten

$$\mathsf{S} \cdot \boldsymbol{k} = 0 \tag{6}$$

involving all the components of the spectral matrix $\mathsf{S}$ and a column vector $\boldsymbol{k}$. For practical usage with the real SVD procedure (see below) we rewrite these equations as a homogeneous system of six real equations,

$$\mathsf{A} \cdot \boldsymbol{k} = 0, \tag{7}$$

where $\mathsf{A}$ is a real matrix $6 \times 3$ obtained by a superposition of the real part ($\Re$) of the spectral matrix over its imaginary part ($\Im$),

$$\mathsf{A} = \begin{pmatrix} \Re S_{11} & \Re S_{12} & \Re S_{13} \\ \Re S_{12} & \Re S_{22} & \Re S_{23} \\ \Re S_{13} & \Re S_{23} & \Re S_{33} \\ 0 & -\Im S_{12} & -\Im S_{13} \\ \Im S_{12} & 0 & -\Im S_{23} \\ \Im S_{13} & \Im S_{23} & 0 \end{pmatrix}. \tag{8}$$

Note that the unknown $\boldsymbol{k}$ can be multiplied by any real coefficient with no effect on (7). This is a consequence of

the fact that from the wave magnetic field we cannot determine the wavelength, but only the wave vector direction. Additionally, we cannot distinguish between two antiparallel wave vector directions because $\boldsymbol{k}$ may be also multiplied by negative numbers in (7). Using (7), we can thus only define $\boldsymbol{k}$ on a hemispheric surface in the wave vector space, and the result can be given in a spherical coordinate system by

$$\begin{aligned} \theta &= \arctan\left(\sqrt{\kappa_1^2+\kappa_2^2}/\kappa_3\right), \\ \phi &= \arctan(\kappa_2/\kappa_1) \quad \text{for } \kappa_1 \geq 0, \\ \phi &= \arctan(\kappa_2/\kappa_1) - \pi \quad \text{for } \kappa_1 < 0, \kappa_2 < 0, \\ \phi &= \arctan(\kappa_2/\kappa_1) + \pi \quad \text{for } \kappa_1 < 0, \kappa_2 \geq 0, \end{aligned} \tag{9}$$

where $\theta$ is a polar angle ranging from $0°$ to $90°$, $\phi$ is an azimuthal angle between $-180°$ and $180°$, and $\kappa_1$, $\kappa_2$, and $\kappa_3$ are Cartesian components of a unity vector $\boldsymbol{\kappa} = \boldsymbol{k}/k$. Since the modulus of $\boldsymbol{\kappa}$ is unity and carries no information, the solution is fully defined by $\theta$ and $\phi$ using (9).

[10] The system (7) has more equations than unknowns. A subset of two independent equations picked up from this system would thus suffice to obtain a unique solution for $\theta$ and $\phi$. This is exactly what is done by some of the existing methods based on the multidimensional spectral analysis of the magnetic field, although they are introduced by different formalisms. The method of *Means* [1972] is based on imaginary parts of three cross-spectra and the procedure is equivalent to solving any two of the last three equations in (7), while replacing the idealized matrix $\mathsf{S}$ by its experimental estimate $\hat{\mathsf{S}}$. The method of *Samson and Olson* [1980, equation (11)] is equivalent to finding a unique solution from another subset of equations selected in (7). Oppositely, the method of *McPherron et al.* [1972] uses the first three equations to perform the eigenanalysis of the real part of the spectral matrix.

[11] By selecting only a part of equations, these methods miss some information contained in the experimental spectral matrix $\hat{\mathsf{S}}$. From the theoretical point of view, this is well justified: The system (7) degenerates into only two independent equations. However, when we use the experimental matrix $\hat{\mathsf{S}}$ it would be true only if $\hat{\mathsf{S}}$ exactly matches its idealized counterpart $\mathsf{S}$. In the appendix we show a special case where this condition holds but in practice it is rarely the case. We only have a limited time series, and the spectral matrices cannot be known without uncertainties due to the spectral analysis. Waves also sometimes contain a significant unpolarized fraction or noise. This was the motivation of *Samson* [1973] who presented different methods of decomposition of the spectral matrix using the eigenanalysis of the spectral matrix without missing any piece of information. This is also our motivation for using the SVD technique.

[12] Let us now replace $\mathsf{A}$ by $\hat{\mathsf{A}}$ in (7) and (8), $\hat{\mathsf{A}}$ being composed of elements of $\hat{\mathsf{S}}$ instead of $\mathsf{S}$ in (8). The modified (7) then reads

$$\hat{\mathsf{A}} \cdot \hat{\boldsymbol{\kappa}} = 0. \tag{10}$$

If this modified set does not degenerate to less than three equations it is not possible to find a vector $\hat{\boldsymbol{\kappa}}$ which simultaneously solves all six equations. Instead, a "solution" can be defined in the least squares sense, it means that we search for a column vector $\hat{\boldsymbol{\kappa}}$ which gives the minimum modulus of a six-dimensional vector $\hat{\mathsf{A}} \cdot \hat{\boldsymbol{\kappa}}$. This can be done without actually having to solve a minimization problem, just using the SVD of the matrix [e.g., *Golub and Van Loan*, 1996],

$$\hat{\mathsf{A}} = \mathsf{U} \cdot \mathsf{W} \cdot \mathsf{V}^{\mathrm{T}}, \tag{11}$$

where $\mathsf{U}$ is a matrix $6 \times 3$ with orthonormal columns, $\mathsf{W}$ is a diagonal matrix $3 \times 3$ of three nonnegative singular values, and $\mathsf{V}^{\mathrm{T}}$ is a matrix $3 \times 3$ with orthonormal rows. Note that the SVD algorithm can often be found in numerical libraries [e.g., *Press et al.*, 1992], and it is very easy to use. This decomposition shows some similarity with the method of *Samson* [1973] based on the eigenanalysis: the squared singular values $\mathsf{W}^2$ are eigenvalues of the matrix $\hat{\mathsf{A}}^{\mathrm{T}} \cdot \hat{\mathsf{A}}$ while the rows of $\mathsf{V}^{\mathrm{T}}$ are the corresponding eigenvectors. Oppositely to *Ladreiter et al.* [1995] who analyzed radio waves by a minimization technique based on a theoretical model of the spectral matrix, our method doesn't implement any explicit minimization procedure and only consist in direct interpretation of the SVD results (11).

[13] The "least squares estimate" for $\hat{\boldsymbol{\kappa}}$ is in fact directly found as the row of $\mathsf{V}^{\mathrm{T}}$ corresponding to the minimum singular value at the diagonal of $\mathsf{W}$. This is a consequence of (11): If we multiply the right-hand side of (11) from the right by $\hat{\boldsymbol{\kappa}}$ defined as the $i$th column of $\mathsf{V}$, the rightmost multiplication gives us a unity vector with all zero components, but the $i$th one (recall that $\mathsf{V}$ has orthonormal columns). Multiplication of this vector with $\mathsf{W}$ then makes a 3 dimensional column vector with all zero components, but the $i$th one which is equal to the $i$th singular value. The leftmost multiplication finally gives us a 6-dimensional vector taken from the $i$th column of $\mathsf{U}$ multiplied by the $i$th singular value. Since $\mathsf{U}$ has orthonormal columns the modulus of the resulting vector is equal to the $i$th singular value. If this is the minimum singular value then we obtain the minimum modulus. Since $\mathsf{V}$ has orthonormal columns, multiplication by any other unit vector $\hat{\boldsymbol{\kappa}}'$ generated by this orthonormal basis would result in a linear combination of orthonormal columns of $\mathsf{U}$ with a higher modulus.

[14] The two other rows of $\mathsf{V}^{\mathrm{T}}$ are perpendicular to the least squares estimate of $\hat{\boldsymbol{\kappa}}$, and thus these rows generate an estimate of the magnetic field polarization plane.

Additionally, an estimate of the direction of the major polarization axis is given by the row of $\mathsf{V}^{\mathrm{T}}$ which corresponds to the maximum singular value. The third direction defined by the last of the orthogonal rows of $\mathsf{V}^{\mathrm{T}}$ corresponds to the minor axis of the magnetic field polarization ellipse. Appendix A shows a simple algebraic example of these results.

[15] If we order the three singular values into an ascending series $w_1$, $w_2$, and $w_3$, we can define the planarity of polarization of the wave magnetic field,

$$F = 1 - \sqrt{w_1/w_3}. \tag{12}$$

Appendix B demonstrates how $F$ is connected to the standard deviations of incoherent noise. A value near to unity means that there are one or two nonzero singular values and the system (10) degenerates into one or two independent equations, respectively. For two nonzero singular values, the above described SVD procedure results then in an exact and unique solution for two variables, as we demonstrate in Appendix A. These two variables can be represented by angles $\theta$ and $\phi$ from (9), using $\hat{\boldsymbol{\kappa}}$ instead of $\boldsymbol{\kappa}$. Moreover, the SVD procedure gives us reasonable results also when $F$ is less than unity. In this case we have three nonzero singular values and the procedure directly gives us a least squares estimate of $\theta$ and $\phi$ using all independent information from (10).

[16] The ratio of the two axes of the polarization ellipse can be defined as

$$L_p = w_2/w_3. \tag{13}$$

When $L_p$ is near to unity, the polarization is circular. When it is near to zero, the polarization is linear. In such a case, there is a single nonzero singular value and the system (10) degenerates to a single equation. As a consequence, we have a plane of possible wave vector directions and a unique solution for $\theta$ and $\phi$ does not exist. Appendix A demonstrates $L_p$ on a simple case of elliptically polarized plane wave.

## 3. Electromagnetic SVD Techniques

[17] With the vector of magnetic field fluctuations the propagation direction cannot be fully determined. As mentioned above, two antiparallel directions cannot be distinguished. We have to use both the magnetic and electric fields to fully determine the wave vector from the Faraday's law (1). For the sake of simplicity we rewrite (1) to

$$\boldsymbol{n} \times \boldsymbol{E} = c\,\boldsymbol{B}, \tag{14}$$

where $\boldsymbol{n} = \boldsymbol{k}c/\omega$ is a dimensionless vector having the modulus of the wave refractive index and the direction of the wave vector, $c$ being the speed of light.

### 3.1. Direct Solution

[18] Suppose the vectors $\boldsymbol{B}$ and $\boldsymbol{E}$ are represented by three magnetic components and three electric components in the same cartesian coordinate system. We can now proceed similarly as in section 2 but instead of using the condition of perpendicularity between $\boldsymbol{B}$ and $\boldsymbol{k}$ we can directly use (14). Multiplying the three complex equations (14) successively by the three cartesian components of $c\boldsymbol{B}^*$, and by the three cartesian components of $\boldsymbol{E}^*$ we have 18 mutually dependent complex equations

$$\sum_{j,k=1}^{3} \epsilon_{ijk}\, E_k\, \zeta_\ell^*\, n_j = c\, B_i\, \zeta_\ell^*, \quad i = 1 \ldots 3,\ \ell = 1 \ldots 6, \tag{15}$$

where $\epsilon_{ijk} = 1$ for $i, j, k = 1, 2, 3$ and for the other two cyclic shifts of this sequence; $\epsilon_{ijk} = -1$ for $i, j, k = 1, 3, 2$ and cyclic shifts; $\epsilon_{ijk} = 0$ otherwise. $\boldsymbol{\zeta}$ is a six-dimensional "electromagnetic" vector

$$\boldsymbol{\zeta} = (cB_1, cB_2, cB_3, E_1, E_2, E_3). \tag{16}$$

Terms $E_k\zeta_\ell^*$ and $cB_i\zeta_\ell^*$ in (15) can be respectively written as selected components $Q_{(k+3)\ell}$ and $Q_{i\ell}$ of a $6 \times 6$ spectral matrix $\mathsf{Q}$. This idealized matrix is composed in the same way as matrix $\mathsf{S}$ in (5), but using the electromagnetic vector $\boldsymbol{\zeta}$ of analytic signals,

$$Q_{ij} = \zeta_i \zeta_j^*. \tag{17}$$

The result can be rewritten as a set of 36 real equations for 3 components of a column vector $\boldsymbol{n}$,

$$\mathsf{A}_{\mathrm{E}} \cdot \boldsymbol{n} = \boldsymbol{b}, \tag{18}$$

where $\mathsf{A}_{\mathrm{E}}$ is a real matrix with 36 rows and 3 columns, and $\boldsymbol{b}$ is a 36-dimensional real column vector. Both are composed in a straightforward manner using (15), (16), and (17) from the components of the $6 \times 6$ spectral matrix $\mathsf{Q}$ but the explicit expressions for $\mathsf{A}_{\mathrm{E}}$ and $\boldsymbol{b}$ would be rather lengthy. We thus only give an example corresponding to the real part of (15) for $i = 1$ and $\ell = 1$; this first row of $\mathsf{A}_E$ is $(0, \Re Q_{61}, -\Re Q_{51})$, and the corresponding row of $\boldsymbol{b}$ is $(Q_{11})$.

[19] The system (18) contains 36 equations for only 3 unknowns. However, in the ideal case of analytic signals these equations are obtained from only six real equations in (14). One of these six equations could be, moreover, eliminated using an appropriate phase factor for the complex amplitudes, and two of them are already contained in the condition $\boldsymbol{E} \cdot \boldsymbol{B} = 0$ which internally bounds the complex electric and magnetic field amplitudes consistent with (1). For analytic signals, the system (18) thus should degenerate into only 3 independent real equations for the three components of $\boldsymbol{n}$.

[20] With real data, the multidimensional spectral analysis at a given frequency results in an estimate $\hat{\mathsf{Q}}$ of the spectral matrix which can be used instead of $\mathsf{Q}$. $\hat{\mathsf{Q}}$ can be obtained in the same manner as in (2), but instead of the estimate of the 3-dimensional vector of magnetic field amplitudes $\hat{\boldsymbol{B}}$ we will now use the 6-dimensional vector $\hat{\boldsymbol{\zeta}}$ of estimates of complex amplitudes of both magnetic and electric fields,

$$\hat{Q}_{ij} = \langle\, \hat{\zeta}_i \hat{\zeta}_j^{*} \,\rangle. \tag{19}$$

The system (18) then becomes

$$\hat{\mathsf{A}}_{\mathrm{E}} \cdot \hat{\boldsymbol{n}} = \hat{\boldsymbol{b}}, \tag{20}$$

where $\hat{\mathsf{A}}_{\mathrm{E}}$ and $\hat{\boldsymbol{b}}$ are composed in the same way as $\mathsf{A}_{\mathrm{E}}$ and $\boldsymbol{b}$, but this time we use components of $\hat{\mathsf{Q}}$ instead of $\mathsf{Q}$.

[21] As discussed in section 2 for equation (10), the system (20) can become overdetermined (degenerating to more than 3 equations). The SVD can be used to estimate $\hat{\boldsymbol{n}}$ which is consistent with all equations (20) in the least squares sense. The matrix $\hat{\mathsf{A}}_{\mathrm{E}}$ can thus be decomposed,

$$\hat{\mathsf{A}}_{\mathrm{E}} = \mathsf{U}_{\mathrm{E}} \cdot \mathsf{W}_{\mathrm{E}} \cdot \mathsf{V}_{\mathrm{E}}^{\mathrm{T}}, \tag{21}$$

where, as in section 2, $\mathsf{U}_{\mathrm{E}}$ is a matrix $36 \times 3$ with three orthonormal columns, $\mathsf{W}_{\mathrm{E}}$ is a diagonal matrix $3 \times 3$ of singular values, and $\mathsf{V}_{\mathrm{E}}^{\mathrm{T}}$ is a matrix $3 \times 3$ with orthonormal rows. It can be proven [e.g., *Press et al.*, 1992] that the least squares solution is then directly given by

$$\hat{\boldsymbol{n}} = \mathsf{V}_{\mathrm{E}} \cdot \mathsf{W}_{\mathrm{E}}^{-1} \cdot \mathsf{U}_{\mathrm{E}}^{\mathrm{T}} \cdot \hat{\boldsymbol{b}}, \tag{22}$$

where $\mathsf{V}_{\mathrm{E}}$ is transposed from $\mathsf{V}_{\mathrm{E}}^{\mathrm{T}}$, and $\mathsf{U}_{\mathrm{E}}^{\mathrm{T}}$ is transposed from $\mathsf{U}_{\mathrm{E}}$. $\mathsf{W}_{\mathrm{E}}^{-1}$ is the diagonal matrix with reciprocal values of the corresponding singular values on the main diagonal.

[22] Using (9) with $\hat{\boldsymbol{n}}$ instead of $\boldsymbol{\kappa}$ we can define the result by the polar angle $\theta$ between $0^\circ$ and $180^\circ$ and the azimuthal angle $\phi$ between $-180^\circ$ and $180^\circ$. The third spherical coordinate, the modulus of $\hat{\boldsymbol{n}}$, now also carries useful information. Due to experimental uncertainties, it must however be used with caution. The electric signals can be affected by an unknown transfer function due to the coupling between the antenna system and the plasma medium. Without going into the details on the experimental problems of electric antennas, we can follow *Gurnett* [1998] and write a general relation between an ideal vector of the analytic complex amplitudes $\boldsymbol{E}$ and a vector of complex amplitudes $\boldsymbol{E}_{\mathbf{Z}}$ affected by the transfer function as

$$\boldsymbol{E}_{\mathrm{Z}} = Z\boldsymbol{E}, \tag{23}$$

where components of $\boldsymbol{E}_{\mathbf{Z}}$ are obtained from ratios of the output voltages of the antenna preamplifiers $V_{\mathrm{out}}$ and the effective lengths of the antennas $L_{\mathrm{eff}}$. $Z$ is then a complex number which could be a function of frequency, and includes also possible uncertainties of the effective lengths. In (23) we assume that the transfer function is the same for all the electric antennas. We can then write $\boldsymbol{E}$ as $\boldsymbol{E}_{\mathbf{Z}}/Z$ and use this expression in (14) and subsequent equations (15) and (16). If $Z$ has no imaginary component (i.e., the transfer function is purely resistive with no phase shift [*Gurnett*, 1998]) we can write $\boldsymbol{n}/Z$ instead of $\boldsymbol{n}$ in (18) and we finally obtain the ratio $\hat{\boldsymbol{n}}/Z$ on the left-hand side of equation (22). The obtained wave vector direction thus remains unaffected. However, the modulus of the vector obtained in that way from (22) represents the ratio of the wave refractive index to the transfer function.

[23] It is important to note that with real data, system (20) can exactly hold only in the case when a single plane wave is present. If the spectral matrix reflects a more complex situation, for instance simultaneous propagation of multiple plane waves, SVD method gives us a least squares estimate of $\hat{\boldsymbol{n}}$, but the system (20) will not exactly hold, i.e., $\hat{\mathsf{A}}_{\mathrm{E}} \cdot \hat{\boldsymbol{n}}$ will not be exactly equal to $\hat{\boldsymbol{b}}$. This property can be used to construct an estimator $F_E$ of the "electromagnetic planarity",

$$F_E = 1 - \sqrt{\frac{\mathcal{N}}{\mathcal{D}}}, \tag{24}$$

where

$$\begin{aligned} \mathcal{N} &= \sum_{i=1}^{36} \left( \hat{\beta}_i - \hat{b}_i \right)^2, \\ \mathcal{D} &= \sum_{i=1}^{36} \left( |\hat{\beta}_i| + |\hat{b}_i| \right)^2, \end{aligned} \tag{25}$$

$\hat{\boldsymbol{\beta}}$ is the left-hand side of (20), $\hat{\boldsymbol{\beta}} = \hat{\mathsf{A}}_{\mathrm{E}} \cdot \hat{\boldsymbol{n}}$, $\hat{\boldsymbol{n}}$ being estimated by the SVD using (22). $F_E$ is unity when system (20) exactly holds, consistent with a presence of a single plane wave. $F_E$ tends to zero with increasing differences of left-hand and right-hand sides of (20). Computer simulations in section 4 will show how this difference is connected to some simplified physical situations.

### 3.2. Transformation to a Homogeneous System

[24] Another possibility how to find an SVD solution of (15) is the transformation into a homogeneous system of equations. We now suppose a more general complex value of $Z$ and we use $\boldsymbol{E}_{\mathbf{Z}} = Z\boldsymbol{E}$ instead of $\boldsymbol{E}$ in (16). After replacing $\boldsymbol{E}$ by $\boldsymbol{E}_{\mathbf{Z}}/Z$ from (23) and after using (17) we obtain expressions $Q_{i\ell}Z$ on the right-hand side of (15). We then have

$$\mathsf{A}_{\mathrm{Z}} \cdot \boldsymbol{n}_{\mathrm{Z}} = 0, \tag{26}$$

where $\boldsymbol{n}_{\mathrm{Z}}$ is a 5-dimensional real vector composed of unknown $\boldsymbol{n}$ (the first three components) and unknown

real and imaginary parts of $Z$ (the last two components). $\mathsf{A}_Z$ is a real matrix $36 \times 5$. It is obtained by adding two new columns to $\mathsf{A}_E$. These columns are $(\Re Q_{i\ell}, -\Im Q_{i\ell})$ for the rows generated by real parts of (15) and $(\Im Q_{i\ell}, \Re Q_{i\ell})$ for the rows generated by imaginary parts of (15).

[25] If we now replace $\mathsf{Q}$ by experimental estimates $\hat{\mathsf{Q}}$ (equation (19)) in the definition of the elements of the matrix $\mathsf{A}_Z$ we obtain the matrix $\hat{\mathsf{A}}_Z$, and equation (26) can be rewritten,

$$\hat{\mathsf{A}}_Z \cdot \hat{\boldsymbol{n}}_Z = 0, \tag{27}$$

where $\hat{\boldsymbol{n}}_Z$ is an unknown 5-dimensional vector.

[26] Following the discussion of (10) in section 2, the homogeneous system of equations (27) can be overdetermined, and SVD finds a least squares estimate of the solution. $\hat{\mathsf{A}}_Z$ can be decomposed to

$$\hat{\mathsf{A}}_Z = \mathsf{U}_Z \cdot \mathsf{W}_Z \cdot \mathsf{V}_Z^{\mathrm{T}}, \tag{28}$$

where the symbols have similar meaning as in (11) and (21); $\mathsf{U}_Z$ is a matrix $36 \times 5$ with five orthonormal columns, $\mathsf{W}_Z$ is a diagonal matrix $5 \times 5$ of singular values, and $\mathsf{V}_Z^{\mathrm{T}}$ is a matrix $5 \times 5$ with orthonormal rows. Then, following the discussion of (11), the unknown vector $\hat{\boldsymbol{n}}_Z$ is obtained as the row of $\mathsf{V}_Z^{\mathrm{T}}$ which corresponds to the minimum singular value from $\mathsf{W}_Z$. Using (9) with the first three components of $\hat{\boldsymbol{n}}_Z$ we can again obtain the polar angle $\theta$ between $0^\circ$ and $180^\circ$ and the azimuthal angle $\phi$ between $-180^\circ$ and $180^\circ$. As in section 3.1, we cannot separate the wave refractive index and the transfer function of electric antennas. Using all five components of $\hat{\boldsymbol{n}}_Z$ we obtain the ratio of refractive index to the absolute value of the transfer function,

$$\hat{n}/|Z| = \sqrt{\left(\hat{n}_{Z1}^2 + \hat{n}_{Z2}^2 + \hat{n}_{Z3}^2\right)} / \sqrt{\left(\hat{n}_{Z4}^2 + \hat{n}_{Z5}^2\right)}. \tag{29}$$

The phase shift connected with the transfer function is defined by the last two components of $\hat{\boldsymbol{n}}_Z$,

$$\begin{aligned} \phi_Z &= \arctan(\hat{n}_{Z5}/\hat{n}_{Z4}) \quad \text{for } \hat{n}_{Z4} \geq 0, \\ \phi_Z &= \arctan(\hat{n}_{Z5}/\hat{n}_{Z4}) + \pi \quad \text{for } \hat{n}_{Z4} < 0. \end{aligned} \tag{30}$$

The same method additionally provides us with another estimator of electromagnetic planarity, obtained now in a similar way as in section 2 from the ratio of the minimum and maximum singular values,

$$F_Z = 1 - \sqrt{w_{Z1}/w_{Z5}}. \tag{31}$$

$F_Z$ varies from 0 to 1. In this case, however, it does not concern the polarization of the wave magnetic field, but it characterizes the consistence of the whole spectral matrix with (14).

### 3.3. Estimation of the Full Spectral Matrix Using Two Electric Antennas

[27] Often, experimental constraints do not allow us to use the data of the full electric field vector, and only two electric components are measured [*Lefeuvre et al.*, 1998; *Cornilleau-Wehrlin et al.*, 1997]. Despite of that, we can still use the SVD analysis methods described in sections 3.1 and 3.2. An estimate of the $6 \times 6$ spectral matrix $\hat{\mathsf{Q}}$ of all field components can be obtained from the spectral matrix of three magnetic and two electric components using the Faraday's law (1) [*Grard*, 1968; *Shawhan*, 1970].

[28] Suppose a $5 \times 5$ spectral matrix $\hat{\mathsf{Q}}^{\mathcal{V}}$,

$$\hat{Q}_{ij}^{\mathcal{V}} = \langle \hat{\xi}_i \hat{\xi}_j^* \rangle, \tag{32}$$

composed of complex amplitudes of the 5 separate signals,

$$\hat{\boldsymbol{\xi}} = \left(c\hat{B}_1, c\hat{B}_2, c\hat{B}_3, \hat{E}_1, \hat{E}_2\right). \tag{33}$$

For a given experimental estimate $\hat{\mathsf{Q}}^{\mathcal{V}}$ (e.g., from a spectral analyzer onboard a spacecraft [*Cornilleau-Wehrlin et al.*, 1997]) we must first reduce the spectral matrix back to estimates of complex amplitudes $\boldsymbol{\xi}$ of separate analytic signals. This procedure can lead to the loss of information because we cannot take into account relative coherence of signals expressed by absolute values of the off-diagonal elements of the spectral matrix (cross-power spectra). Modulus of each signal is defined as a square root of the corresponding diagonal element (auto-power spectrum). The phase shift of each signal is estimated by a least squares method from all relevant cross-spectra. The modulus and the phase shift define the complex amplitude.

[29] The procedure needs three cartesian components of the magnetic field and two mutually perpendicular electric components. If the directions of the two electric antennas are not perpendicular a correction of their complex amplitudes can be done. The complex amplitudes of the three magnetic components are then transformed to the Cartesian system defined by the two measured electric components $E_x$ and $E_y$. Next, real and imaginary parts of the third electric component $E_z$ are calculated from equations

$$\begin{aligned} \Re \boldsymbol{E} \cdot \Re \boldsymbol{B} &= 0, \\ \Im \boldsymbol{E} \cdot \Im \boldsymbol{B} &= 0, \end{aligned} \tag{34}$$

respectively. These equations are a consequence of (1). Finally, the $6 \times 6$ spectral matrix $\hat{\mathsf{Q}}$ can be reconstituted using (16) and (17).

[30] Since this $\hat{\mathsf{Q}}$ is now created artificially consistent with (1) and hence with (14) and (18), the electromagnetic planarity estimators $F_E$ (equation (24)) and

$F_Z$ (equation (31)) do not reflect the real polarization properties of the original data. To obtain an electromagnetic planarity estimator based on the measurement using only two electric antennas we can, however, still use a very similar method to that described in (24) for the estimator $F_E$. Equation (14) can be written in cartesian coordinates defined by the plane of the two electric antennas. From these three complex equations we pick up only the single equation where the two available electric components are on the left-hand side, and we drop the two other equations containing the electric component which is not measured. Similarly as in (15) we can write a system of 5 complex equations for analytic signals ideally consistent with (14),

$$E_1\xi_\ell^*\, n_2 - E_2\xi_\ell^*\, n_1 = c\, B_3\, \xi_\ell^*, \quad \ell = 1 \ldots 5, \qquad (35)$$

where terms $E_k\xi_\ell^*$ and $cB_3\xi_\ell^*$ can be respectively written as selected components $Q^{\mathcal{V}}_{(k+3)\ell}$ and $Q^{\mathcal{V}}_{3\ell}$ of a $5 \times 5$ spectral matrix $\mathsf{Q}^{\mathcal{V}}$. This idealized matrix is composed in the same way as matrix $\mathsf{Q}$ in (17), but using the vector $\boldsymbol{\xi}$ of analytic signals,

$$Q^{\mathcal{V}}_{ij} = \xi_i\xi_j^*. \qquad (36)$$

The electromagnetic planarity estimator for the experimental spectral matrix (32) can be then written,

$$F_V = 1 - \sqrt{\frac{\mathcal{N}_{\mathcal{V}}}{\mathcal{D}_{\mathcal{V}}}} \qquad (37)$$

where

$$\begin{aligned} \mathcal{N}_{\mathcal{V}} &= \sum_{\ell=1}^{10} \left( \hat{Q}^{\mathcal{V}}_{4\ell}\, \hat{n}_2 - \hat{Q}^{\mathcal{V}}_{5\ell}\, \hat{n}_1 - \hat{Q}^{\mathcal{V}}_{3\ell} \right)^2, \\ \mathcal{D}_{\mathcal{V}} &= \sum_{\ell=1}^{10} \left( |\hat{Q}^{\mathcal{V}}_{4\ell}\, \hat{n}_2 - \hat{Q}^{\mathcal{V}}_{5\ell}\, \hat{n}_1| + |\hat{Q}^{\mathcal{V}}_{3\ell}| \right)^2, \end{aligned} \qquad (38)$$

$\hat{\boldsymbol{n}}$ being estimated by the SVD method (22) from the $6 \times 6$ matrix $\hat{\mathsf{Q}}$ reconstituted from $\hat{\mathsf{Q}}^{\mathcal{V}}$ using (34).

[31] Note that when we have the data of three magnetic and a single electric antennas the above described method cannot be used. Under some conditions, we are however able to estimate the hemisphere of the wave propagation [*Santolík and Parrot*, 1999]. The wave distribution function (WDF) methods (see below) can also determine the hemisphere of propagation as shown for instance by *Lefeuvre et al.* [1992].

## 4. Tests With Simulated Data

[32] In order to verify the functionality of the above described methods we have done throughout tests using simulated data. In this section we will present two examples of simulations using the concept of the WDF which has been introduced by *Storey and Lefeuvre* [1979] to describe the situations when the waves simultaneously propagate at more than one wave vector direction. Assumption on the presence of a single plane wave with a single wave vector direction was used in derivation of the above described SVD methods. It is therefore important to know how the results of the analysis behave when this assumption is not valid.

[33] We proceed as follows. First, we choose parameters of the anisotropic plasma medium, wave frequencies, and propagation modes corresponding to observations [*Santolík et al.*, 2001] in the high-altitude auroral region. We define the plasma frequency $f_p$ = 10.5 kHz, the electron cyclotron frequency is $f_g$ = 27 kHz, the wave frequency of 4.5 kHz for the first simulation of Z-mode waves, and the wave frequency of 9 kHz for the second simulation of whistler mode waves.

[34] Next, we choose a wave vector direction $\boldsymbol{\kappa}$ and we calculate theoretical vectors of complex amplitudes of wave electric and magnetic fields using the theory of the cold magnetized plasma [e.g., *Stix*, 1992]. Aiming to simulate the data of *Santolík et al.* [2001], we use three orthogonal magnetic antennas and two electric antennas, we project the vectors of complex amplitudes to the predefined directions of antennas, and we form theoretical spectral matrices $\mathsf{S}$ and $\mathsf{Q}^{\mathcal{V}}$ following (5) and (36), respectively.

[35] Finally, we use these theoretical spectral matrices, calculated for different $\boldsymbol{\kappa}$ as the integration kernels in the equation of the direct problem of the WDF [*Storey and Lefeuvre*, 1979],

$$\begin{aligned} \check{S}_{ij} &= \int S_{ij}(\boldsymbol{\kappa}) G(\boldsymbol{\kappa}) d\boldsymbol{\kappa}^2, \\ \check{Q}^{\mathcal{V}}_{ij} &= \int Q^{\mathcal{V}}_{ij}(\boldsymbol{\kappa}) G(\boldsymbol{\kappa}) d\boldsymbol{\kappa}^2, \end{aligned} \qquad (39)$$

where $\int d\kappa^2$ denotes integration over the surface of the unit sphere, $G(\boldsymbol{\kappa})$ is the WDF, and $\check{\mathsf{S}}$, $\check{\mathsf{Q}}^{\mathcal{V}}$ are model spectral matrices at the given frequency. These matrices are used instead of experimental spectral matrices $\hat{\mathsf{S}}$ and $\hat{\mathsf{Q}}^{\mathcal{V}}$ as the input information for the SVD analysis methods. We compare the results with the methods of *Means* [1972] and *Samson* [1973] used for the same input data. We use a Cartesian coordinate system connected with the DC magnetic field. For instance, angles $\theta$ and $\phi$ define the deviation of the wave vector from the DC magnetic field, and the wave vector azimuth, respectively.

[36] In Figure 1 we show results of a simulation of the Z-mode waves at a frequency of 4.5 kHz. We suppose that the waves propagate in a divergent beam of wave vectors which is described as a Gaussian peak on the WDF (a model defined as "GP" by *Santolík and Parrot* [2000]). The central direction of the beam is defined by

$\theta_0 = 50°$ and $\phi_0 = 50°$ and its angular width ($\Delta$) varies from zero to 90°. For $\Delta = 0°$, the beam collapses to a single plane wave at $\theta_0 = 50°$ and $\phi_0 = 50°$. For $\Delta \rightarrow \infty$, the waves simultaneously propagate at all directions with $\theta \leq 90°$.

[37] Figure 1a shows that the angle $\theta$ estimated by the method of *Means* [1972] (dotted line) rapidly decreases from the central value $\theta_0 = 50°$ with a growing width of the peak. The estimates done by the magnetic SVD method (solid line) and by the method of *Samson* [1973] (dash-dot line) give larger $\theta$ than the central value, the method of *Samson* [1973] being closer to $\theta_0$. The electromagnetic SVD method gives a result which is always nearest to the central direction (dashed line). The $\phi$ values (Figure 1b) are estimated very near to the original central direction $\phi_0 = 50°$ by all the methods for all $\Delta$. The electromagnetic SVD method (dashed line) deviates at maximum by one degree, the other methods giving always exactly $\phi_0$. The index of refraction (Figure 1c) from the electromagnetic SVD method is always the same as for a plane wave at the central direction. Both planarity estimates (Figure 1d) decrease with increasing $\Delta$, the electromagnetic planarity $F_V$ (equation (37)) being significantly less sensitive to the peak width than the planarity of the polarization of magnetic field fluctuations $F$ (equation (12)).

[38] The assumption on the presence of a single plane wave is also invalid when the waves simultaneously propagate in both hemispheres for $\theta \leq 90°$ and $\theta > 90°$. Figure 2 shows simulation results for such a case. We simulate data corresponding to whistler mode waves at a frequency of 9 kHz. We use the same parameters of the cold plasma model as in the first simulation. The theoretical spectral matrix is calculated for two plane waves which simultaneously propagate in mutually antiparallel directions placed not far from the resonance cone at $\theta_R = 29°$. The two direction are defined respectively by $\theta_1 = 28°$, $\phi_1 = 10°$, and $\theta_2 = 152°$, $\phi_2 = -170°$. We gradually change the percentage ($p$) of energy density carried by each of the two waves. When $p = 0\%$, only the wave at $\theta_1 = 28°$, $\phi_1 = 10°$ propagates. Oppositely, a single plane wave at $\theta_2 = 152°$, $\phi_2 = -170°$ propagates when $p = 100\%$. If $p = 50\%$ the same energy density is placed into the two antiparallel waves.

[39] Obtained results strictly reproduce the properties of the wave with higher energy density. At $p = 50\%$ the results of the electromagnetic SVD method (sections 3.1 and 3.3) switch between the two antiparallel directions (Figures 2a and 2b, dashed line). As discussed in section 2 the results obtained without considering the wave electric field (solid line for the three methods: *Means* [1972], *Samson* [1973], and section 2) always indicate the hemisphere where $\theta \leq 90°$, and, as the two simulated wave vectors are antiparallel, no change is observed at $p = 50\%$. No effect is observed on the estimate of the refractive index (Figure 2c). The presence of waves in both hemispheres is indicated by a smooth decrease of the electromagnetic planarity $F_V$ (equation (37)) down to zero at $p = 50\%$ (Figure 2d, dashed line). As the wave magnetic field does not reflect the presence of the two antiparallel waves at all, the estimate of the magnetic planarity $F$ (equation (12)) is always unity (Figure 2d, solid line).

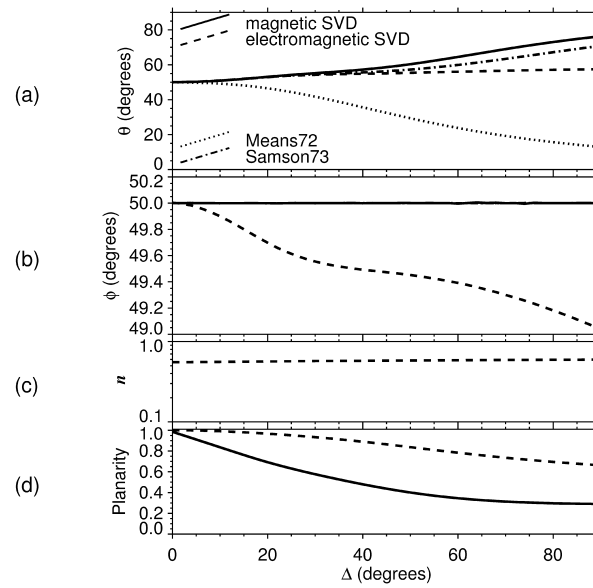


**Figure 1.** Analysis of the influence of the plane wave hypothesis for a beam of Z-mode waves. Simulated results are given in four panels as a function of the width $\Delta$ of a Gaussian wave distribution function. (a) Polar angle $\theta$ estimated by the method of *Means* [1972], by the method of *Samson* [1973], by the magnetic SVD method from section 2, and by the electromagnetic SVD method from section 3.1 with the electric field vector completed using the procedure described in section 3.3; (b) Azimuthal angle $\phi$ estimated by the same four methods; (c) Refractive index $n$ estimated by the SVD method from sections 3.1 and 3.3; (d) Planarity $F$ (equation (12)—solid line) and electromagnetic planarity $F_V$ (equation (37)—dashed line) from sections 2 and 3.3, respectively.

## 5. Analysis of a Multicomponent Measurement in the High-Altitude Auroral Region

[40] Figure 3 presents an example of results of the SVD analysis of natural emissions measured in the high-altitude auroral region [*Santolík et al.*, 2001]. The data have been recorded on 9 November 1996, at 2320:10 h

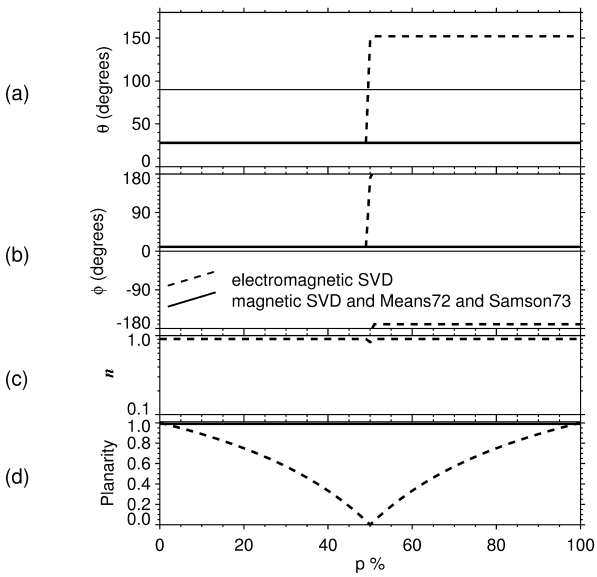


**Figure 2.** Analysis of simulated whistler mode waves simultaneously propagating in two antiparallel directions at 9 kHz. Results plotted as a function of the percentage $p$ of the energy density of the up-coming wave. The panels and line styles are the same as in Figure 1.

UT by the MEMO device onboard the INTERBALL-2 satellite. The satellite was located at an invariant latitude of 73.8°, on 0310 h MLT and at an altitude of 18,038 km. The electric and magnetic spectra show emissions with both lower-frequency and higher-frequency cutoffs (see Figures 3e and 3f). The polarization analysis indicates that the majority of waves in the frequency band 3.6–5 kHz above the lower-frequency cutoff propagate in the left-hand polarized Z-mode, and that the waves at frequencies above 6 kHz and below the higher-frequency cutoff at 10.5 kHz mainly propagate in the right-hand polarized whistler mode [*Santolík et al.*, 2001, Figure 1].

[41] The analysis results (Figures 3a–3d) are shown only for frequencies where both the sums of power spectral densities of the wave electric field components ($E_S$) and magnetic field components ($B_S$) are well above the background noise ($B_S > 1.4 \cdot 10^{-10}$ nT$^2$/Hz, $E_S > 10^{-3}$ mV$^2$/m$^2$/Hz). We use only two methods: the magnetic SVD method from section 2 (solid line), and the electromagnetic SVD method from section 3.1 with the electric field vector completed by the method described in section 3.3 (dashed line). Looking first at the results for the wave vector direction, we can see that in the Z-mode band below 5 kHz the waves propagate in the hemisphere where $\theta \leq 90°$ (Figure 3a), and that the $\theta$ values rapidly grow with frequency from 20°–40° up to 90°. The $\phi$ values (Figure 3b) are between 40° and 90°. There are some differences between the results of the two methods which will be discussed later on. In the whistler mode band above 6 kHz, the electromagnetic SVD method shows that the waves propagate mainly in the hemisphere where $\theta > 90°$. $\theta$ is between 100° and 140° with a short excursion below 90° around 9 kHz, $\phi$ being near 40°. The SVD method from section 2 cannot determine the hemisphere of propagation, but gives similar results if we inverse the wave vector direction,

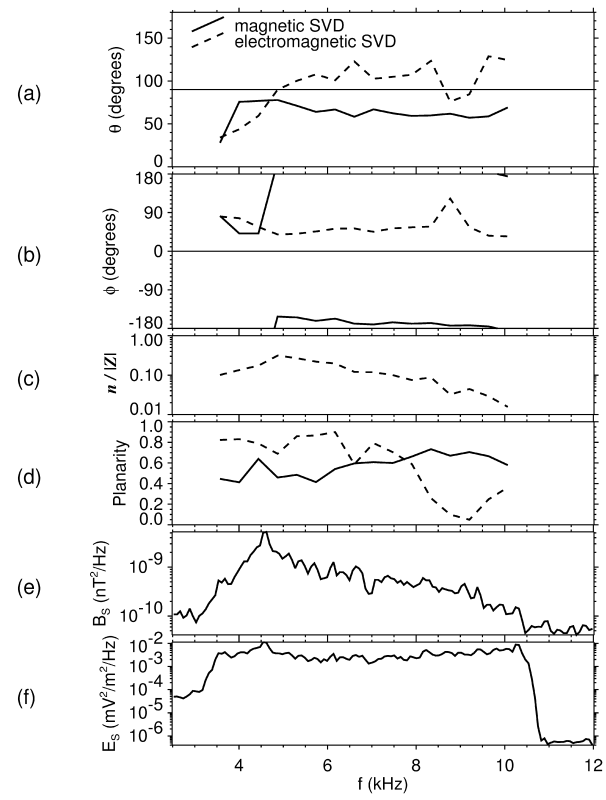


**Figure 3.** Analysis of Z-mode and whistler mode VLF emissions in the frequency interval 2.5–12 kHz. Data were recorded by the MEMO device onboard INTERBALL-2 on 9 November 1996 at 2320:10 h UT. Panels (a)–(d) show the same parameters as in Figure 1. (e) Sum of the power spectra of the three orthogonal magnetic components; (f) sum of the power spectra of electric signals measured by two orthogonal antennas. The same line styles as in Figure 1 are used for the results of the two SVD methods, the magnetic SVD method from section 2 (solid line), and the electromagnetic SVD method from section 3.1 with the electric field vector completed by the method described in section 3.3 (dashed line).

except for the $\phi$ values which are near 180°. The values of $n/|Z|$ grow from 0.1 to 0.3 in the Z-mode band, and decrease to 0.02 in the whistler mode band.

[42] The results for the wave vector direction can be explained by the complexity of the wave fields reflected by the two estimators of the planarity of polarization. The magnetic planarity $F$ (12) from section 2 is lower in the Z-mode band below 5 kHz. This indicates that the waves do not propagate as a single plane wave. Dispersion of wave vector directions to a large WDF also explains the differences of $\theta$ values obtained by the two different methods in this band. The electromagnetic planarity $F_V$ (37), however, is rather high in this band. As shown by analysis of simulated data in the preceding section (Figure 1), the electromagnetic SVD method indicate in such a case an average wave vector direction of observed waves.

[43] The electromagnetic planarity $F_V$ (37) substantially decreases in the whistler mode band above 6 kHz, and goes nearly to zero around 9 kHz. As indicated by another analysis of simulated data described in the preceding section (Figure 2), this is probably due to simultaneous presence of waves in both hemispheres of propagation (for $\theta \leq 90°$ and $\theta > 90°$). The hemisphere of propagation just below the higher-frequency cutoff of the whistler mode band at 10.5 kHz is in agreement with the Poynting vector directions determined from the same data (not shown). Further interpretation of these results in terms of the possible sources of the observed emissions is beyond the scope of this paper and is done elsewhere [*Santolík et al.*, 2001].

## 6. Summary

[44] We have presented a detailed description of several newly developed methods for propagation analysis of electromagnetic plasma waves. All these methods are based on the singular value decomposition (SVD) technique which takes into account all information contained in a spectral matrix. With the spectral matrix of three magnetic components the SVD technique allows us to simultaneously determine the wave vector direction in a single hemisphere (without distinguishing two antiparallel directions), the direction of axes of the polarization ellipse, its the ratio of their lengths, and the planarity of polarization. With the spectral matrix of three magnetic components and two or three electric components, the SVD technique allows us to determine the fully defined wave vector direction, the ratio of the refractive index and the absolute value of the transfer function of electric antennas, the phase shift induced by this transfer function, and the electromagnetic planarity.

[45] With the analysis of simulated whistler mode and Z-mode waves we have shown that (a) the SVD methods (especially the electromagnetic ones) better reflect central direction of a beam of wave vectors of simultaneously propagating waves. (b) The electromagnetic planarity estimator can be used to indicate cases when the waves simultaneously propagate in two opposite hemispheres. The analysis of natural whistler mode and Z-mode emissions in the high-altitude auroral region shows that the SVD methods give consistent results, and that they may serve as a useful tool for propagation analysis of multicomponent measurements of plasma waves made onboard artificial satellites.

[46] All the above presented methods are contained in the computer program PRASSADCO [*Santolík*, 2000] designed primarily for the analysis of data of the STAFF-SA devices onboard the Cluster satellites [*Cornilleau-Wehrlin et al.*, 1997]. The results shown in the present paper have been obtained by this program.

## Appendix A: Algebraic SVD Solution for the Magnetic Spectral Matrix of a Totally Polarized Wave

[47] Let us suppose that the wave is totally polarized in a plane defined by axes $x_1$ and $x_2$ of a cartesian coordinate system, the major axis of the polarization ellipse being along $x_1$. The corresponding components of the magnetic field then fluctuate as sine waves,

$$\begin{aligned} \mathcal{B}_1(t) &= a\cos(2\pi ft), \\ \mathcal{B}_2(t) &= b\sin(2\pi ft), \\ \mathcal{B}_3(t) &= 0, \end{aligned} \tag{A1}$$

where $f$ it the frequency, $t$ is time, and $a$ and $b$ are real amplitudes corresponding respectively to the major and minor axis of the polarization ellipse ($a \geq b$). The particular choice of coordinate system doesn't represent any restriction, and a generalization for an arbitrary system will be shown later on.

[48] Suppose also that the signals are sampled at times separated by equal time intervals $\tau$, resulting in time series of $M$ samples $\mathcal{B}_1(m\tau)$ and $\mathcal{B}_2(m\tau)$, $m = 1 \ldots M$. To facilitate further discussion we will also suppose that one quarter of the period of the sine wave exactly matches an entire number of sampling intervals,

$$\tau = \frac{1}{4Kf}, \tag{A2}$$

where $K$ is a positive entire number. This represents the first principal assumption allowing us to obtain simple algebraic expressions for the results of the spectral analysis. Similar analysis would be more complicated for a general case which does not necessarily satisfy the condition (A2). However, for $K \gg 1$ we expect that the results would be very close to what is obtained below.

[49] Choosing the discrete Fourier transform method of the spectral analysis of real signals $\mathcal{B}_1$ and $\mathcal{B}_2$ we obtain the estimates $\hat{B}_1$ and $\hat{B}_2$ of the complex amplitudes at an angular frequency $\omega = 2\pi f$,

$$\begin{aligned}
\Re\hat{B}_1 &= \frac{2}{M}\sum_{m=1}^{M} a\,\cos^2(\omega m\tau),\\
\Im\hat{B}_1 &= \frac{2}{M}\sum_{m=1}^{M} a\,\sin(\omega m\tau)\cos(\omega m\tau),\\
\Re\hat{B}_2 &= \frac{2}{M}\sum_{m=1}^{M} b\,\cos(\omega m\tau)\sin(\omega m\tau),\\
\Im\hat{B}_2 &= \frac{2}{M}\sum_{m=1}^{M} b\,\sin^2(\omega m\tau).
\end{aligned} \tag{A3}$$

We have assumed here a rectangular weighting window which is unity inside the closed time interval between $\tau$ and $M\tau$ and zero outside.

[50] Assume further that the duration of the time series of samples exactly matches an entire number $Q$ of wave periods,

$$M\tau = Q/f. \tag{A4}$$

This is the second principal assumption, which in a general case becomes approximately valid for $Q \gg 1$. $\Im\hat{B}_1$ and $\Re\hat{B}_2$ then vanish, $\Re\hat{B}_1 = a$ and $\Im\hat{B}_2 = b$. Since these estimates are always the same for all the successive series of $M$ samples of magnetic field components (A1) satisfying the conditions (A2) and (A4), the averaging in the calculation (2) of the spectral matrix has no effect.

[51] Spectral matrix thus only has four nonzero elements, $S_{11} = a^2$, $S_{22} = b^2$, $S_{12} = -\iota ab$, and $S_{21} = \iota ab$. The SVD of matrix A from (11) then reads

$$\mathsf{A} = \mathsf{U}\cdot\mathsf{W}\cdot\mathsf{V}^{\mathrm{T}}, \text{ where} \tag{A5}$$

$$\mathsf{A} = \begin{pmatrix} a^2 & 0 & 0\\ 0 & b^2 & 0\\ 0 & 0 & 0\\ 0 & ab & 0\\ -ab & 0 & 0\\ 0 & 0 & 0 \end{pmatrix}, \tag{A6}$$

$$\mathsf{U} = \begin{pmatrix} a/\sqrt{a^2+b^2} & 0 & 0\\ 0 & b/\sqrt{a^2+b^2} & 0\\ 0 & 0 & 1\\ 0 & a/\sqrt{a^2+b^2} & 0\\ -b\sqrt{a^2+b^2} & 0 & 0\\ 0 & 0 & 0 \end{pmatrix}, \tag{A7}$$

$$\mathsf{W} = \begin{pmatrix} a\sqrt{a^2+b^2} & 0 & 0\\ 0 & b\sqrt{a^2+b^2} & 0\\ 0 & 0 & 0 \end{pmatrix}, \text{ and} \tag{A8}$$

$$\mathsf{V} = \begin{pmatrix} 1 & 0 & 0\\ 0 & 1 & 0\\ 0 & 0 & 1 \end{pmatrix}. \tag{A9}$$

[52] We can see that the diagonal matrix $\mathsf{W}$ contains two nonzero singular values. The planarity from (12) is thus $F = 1$ and the ellipticity from (13) $L_p = a/b$. That means we retrieve the original ratio of the two axes of the polarization ellipse. Moreover, the last column of the matrix $\mathsf{V}$ (the column corresponding to the position of the zero singular value in $\mathsf{W}$) gives us the wave vector direction along the axis $x_3$, which is perpendicular to the plane of polarization. In that plane, the direction $x_1$ corresponds to the major axis (the column of $\mathsf{V}$ corresponding to the largest singular value $a/\sqrt{a^2+b^2}$). The result in (A5) thus reflects all properties of the original model (A1).

## Appendix B: Algebraic SVD Solution for the Magnetic Spectral Matrix of a Random Noise

[53] Supposing now that the cartesian components of the magnetic field fluctuate as a random noise, the samples $\mathcal{B}_i(m\tau)$ can be defined as independent random variables with zero mean values and finite standard deviations. Supposing further that these standard deviations are constant for the $i$th cartesian component, we can define for all the samples of $\mathcal{B}_1(t)$, $\mathcal{B}_2(t)$, and $\mathcal{B}_3(t)$ the standard deviations $a$, $b$, and $c$, respectively, and choose that $a \geq b \geq c$. Again, that particular choice of coordinate system doesn't represent any loss of generality, as we will demonstrate later on.

[54] Choosing the discrete Fourier transform method for the spectral analysis of these real signals we have,

$$\begin{aligned}
S_{ij}(\omega) = \Bigg\langle &\sum_{k=1}^{M}\mathcal{B}_i(k\tau)\exp(\iota\omega k\tau)\\
&\cdot\sum_{\ell=1}^{M}\mathcal{B}_j(\ell\tau)\exp(-\iota\omega\ell\tau)\Bigg\rangle,
\end{aligned} \tag{B1}$$

giving

$$\begin{aligned}
S_{ij}(\omega) = &\sum_{k,\ell=1}^{M}\exp[\iota\omega(k-\ell)\tau]\\
&\cdot\frac{1}{P}\sum_{m=1}^{P}\mathcal{B}_i(k\tau+mM)\mathcal{B}_j(\ell\tau+mM),
\end{aligned} \tag{B2}$$

where $\iota$ is $\sqrt{-1}$, and the symbols $\langle\ \rangle$ were replaced by averaging results obtained from $P$ successive time series. Product $M\tau$ was chosen so that it covers an entire number $Q$ of wave periods according to (A4).

[55] For large $P$ the innermost sum in (B2) is nonzero only for $i = j$ and $\ell = k$. In that case the result is the variance of the respective component. Otherwise different terms of the innermost sum cancel out since each sample is an independent random variable. The resulting spectral matrix thus only has three nonzero elements, the auto-spectra $S_{11} = a^2$, $S_{22} = b^2$, and $S_{33} = c^2$. The SVD of matrix A from (11) then reads

$$\mathsf{A} = \mathsf{U} \cdot \mathsf{W} \cdot \mathsf{V}^{\mathrm{T}}, \text{ where} \tag{B3}$$

$$\mathsf{A} = \begin{pmatrix} a^2 & 0 & 0 \\ 0 & b^2 & 0 \\ 0 & 0 & c^2 \\ 0 & 0 & 0 \\ 0 & 0 & 0 \\ 0 & 0 & 0 \end{pmatrix}, \tag{B4}$$

$$\mathsf{U} = \begin{pmatrix} 1 & 0 & 0 \\ 0 & 1 & 0 \\ 0 & 0 & 1 \\ 0 & 0 & 0 \\ 0 & 0 & 0 \\ 0 & 0 & 0 \end{pmatrix}, \tag{B5}$$

$$\mathsf{W} = \begin{pmatrix} a^2 & 0 & 0 \\ 0 & b^2 & 0 \\ 0 & 0 & c^2 \end{pmatrix}, \text{ and} \tag{B6}$$

$$\mathsf{V} = \begin{pmatrix} 1 & 0 & 0 \\ 0 & 1 & 0 \\ 0 & 0 & 1 \end{pmatrix}. \tag{B7}$$

[56] We can see that the diagonal matrix $\mathsf{W}$ contains three nonzero singular values equal to variances of noise in the respective components. The planarity from (12) is then $F = 1 - c/a$, and reflects the ratio of minimum to maximum standard deviation of noise.

## Appendix C: Transformation of Algebraic SVD Solutions to an Arbitrary Coordinate System

[57] If we now use arbitrary cartesian coordinate system defined by a transformation matrix $\mathsf{T}$,

$$\mathcal{B}'_i = \sum_{k=1}^{3} T_{ik} \mathcal{B}_k, \tag{C1}$$

where $\mathcal{B}'_i$ is a vector component in the new system, the transformed spectral matrix will be $\mathsf{S}' = \mathsf{T} \cdot \mathsf{S} \cdot \mathsf{T}^{\mathrm{T}}$. In this case the transformed matrix A will be

$$\mathsf{A}' = \begin{pmatrix} \mathsf{T} & 0 \\ 0 & \mathsf{T} \end{pmatrix} \cdot \mathsf{A} \cdot \mathsf{T}^{\mathrm{T}}, \tag{C2}$$

and its SVD transforms as

$$\mathsf{A}' = \mathsf{U}' \cdot \mathsf{W} \cdot \mathsf{V}'^{\mathrm{T}}, \text{ where}$$

$$\mathsf{U}' = \begin{pmatrix} \mathsf{T} & 0 \\ 0 & \mathsf{T} \end{pmatrix} \cdot \mathsf{U}, \tag{C3}$$

$$\mathsf{V}' = \mathsf{T} \cdot \mathsf{V}.$$

Since $\mathsf{V}$ is a unity matrix in (A5), we have $\mathsf{V}' = \mathsf{T}$, and the columns of $\mathsf{V}'$ are again the vectors defining the axes of the polarization ellipse and the wave vector direction in the new coordinate system. The parameters $F$ and $L_p$ do not change since the matrix of singular values $\mathsf{W}$ remains unchanged after the transformation.

[58] **Acknowledgments.** This work was supported by the French–Czech program Barrande 98039/98055 and by the international program of scientific cooperation (PICS) 469 with the joint Czech Grant Agency grant 205/01/1064. O. Santolík acknowledges the support of the MSM 113200004 and GAUK 169/2002 projects.

## References

Cornilleau-Wehrlin, N., et al., The Cluster spatio-temporal analysis of field fluctuations (STAFF) experiment, *Space Sci. Rev.*, *79*, 107–136, 1997.

Golub, G. H., and C. F. Van Loan, *Matrix Computations*, Johns Hopkins Univ. Press, Baltimore, Md., 1996.

Grard, R., Interprétation de mesures de champ électromagnétique T.B.F. dans la magnétosphère, *Ann. Geophys.*, *24*, 955–971, 1968.

Gurnett, D. A., Principles of space plasma wave instrument design, in *Measurement Techniques in Space Plasmas: Fields*, *Geophys. Monogr.*, vol. 103, pp. 121–136, AGU, Washington, D. C., 1998.

Gurnett, D. A., et al., The polar plasma wave instrument, *Space Sci. Rev.*, *71*, 597–622, 1995.

Ladreiter, H. P., P. Zarka, A. Lecacheux, W. Macher, H. O. Rucker, R. Manning, D. A. Gurnett, and W. S. Kurth, Analysis of electromagnetic wave direction finding performed by spaceborne antennas using singular-value decomposition techniques, *Radio Sci.*, *30*, 1699–1712, 1995.

Lefeuvre, F., J. L. Rauch, D. Lagoutte, J. J. Berthelier, and J. C. Cerisier, Propagation characteristics of dayside low-altitude hiss: Case studies, *J. Geophys. Res.*, *97*, 601–620, 1992.

Lefeuvre, F., M. Parrot, J. L. Rauch, B. Poirier, A. Masson, and M. Mogilevsky, Preliminary results from the MEMO multi-

component measurements of waves on-board INTERBALL 2, *Ann. Geophys.*, *16*, 1117–1136, 1998.

McPherron, R. L., C. T. Russel, and P. J. Coleman Jr., Fluctuating magnetic fields in the magnetosphere, 2, ULF waves, *Space Sci. Rev.*, *13*, 411–454, 1972.

Means, J. D., Use of the three-dimensional covariance matrix in analyzing the polarization properties of plane waves, *J. Geophys. Res.*, *77*, 5551–5559, 1972.

Press, W. H., B. P. Flannery, S. A. Teukolsky, and W. T. Vetterling, *Numerical Recipes*, Cambridge Univ. Press, New York, 1992.

Priestley, M. B., *Spectral Analysis and Time Series*, Academic, San Diego, Calif., 1989.

Rezeau, L., A. Roux, and C. T. Russell, Characterization of small-scale structures at the magnetopause from ISEE measurements, *J. Geophys. Res.*, *98*, 179–186, 1993.

Samson, J. C., Descriptions of the polarization states of vector processes: Applications to ULF magnetic fileds, *Geophys. J. R. Astron. Soc.*, *34*, 403–419, 1973.

Samson, J. C., and J. V. Olson, Some comments on the descriptions of the polarisation states of waves, *Geophys. J. R. Astron. Soc.*, *61*, 115–129, 1980.

Santolík, O., Propagation Analysis of Staff-SA Data with Coherency Tests, *LPCE/NTS/073.A*, Lab. Phys. Chimie Environ./CNRS, Orléans, France, 2000.

Santolík, O., and M. Parrot, Case studies on wave propagation and polarization of ELF emissions observed by Freja around the local proton gyro-frequency, *J. Geophys. Res.*, *104*, 2459–2476, 1999.

Santolík, O., and M. Parrot, Application of wave distribution function methods to an ELF hiss event at high latitudes, *J. Geophys. Res.*, *105*, 18,885–18,894, 2000.

Santolík, O., F. Lefeuvre, M. Parrot, and J. L. Rauch, Propagation of Z-mode and whistler-mode emissions observed by Interball 2 in the nightside auroral region, *J. Geophys. Res.*, *106*, 21,137–21,146, 2001.

Shawhan, S. D., The use of multiple receivers to measure the wave characteristics of very-low-frequency noise in space, *Space Sci. Rev.*, *10*, 689–736, 1970.

Stix, T. H., *Waves in Plasmas*, Am. Inst. of Phys., New York, 1992.

Storey, L. R. O., and F. Lefeuvre, The analysis of 6-component measurement of a random electromagnetic wave field in a magnetoplasma, 1, The direct problem, *Geophys. J. R. Astron. Soc.*, *56*, 255–270, 1979.

---

F. Lefeuvre and M. Parrot, Laboratoire de Physique et Chimie de l'Environnement, Centre National de la Recherche Scientifique, 3A, Avenue de la Recherche Scientifique, F-45071 Orléans cedex 02, France. (lefeuvre@cnrs-orleans.fr; mparrot@cnrs-orleans.fr)

O. Santolík, Faculty of Mathematics and Physics, Charles University, V Holešovičkách 2, CZ-18000 Prague, Czech Republic. (ondrej.santolik@mff.cuni.cz)